Organic characterisation of cave drip water by LC-OCD and fluorescence analysis

Rutlidge, Helen; Andersen, Martin S.; Baker, Andy; Chinu, Khorshed J.; Cuthbert, Mark O.; Jex, Catherine N.; Marjo, Christopher E.; Markowska, Monika; Rau, Gabriel C.

DOI:
10.1016/j.gca.2015.05.042

Organic characterisation of cave drip water by LC-OCD and fluorescence analysis

Helen Rutlidge,[a,b,*] Martin S. Andersen,[c,] Andy Baker,[b,] Khorshed J. Chinu,[a] Mark O. Cuthbert,[c,d,] Catherine Jex,[b,] Christopher E. Marjo,[a,] Monika Markowska,[b,e,] Gabriel C. Rau[c]

[a] Solid State and Elemental Analysis Unit, Mark Wainwright Analytical Centre, UNSW Australia, Kensington, NSW, Australia 2052

[b] Connected Waters Initiative Research Centre, UNSW Australia, Kensington, NSW, Australia 2052

[c] Connected Waters Initiative Research Centre, UNSW Australia, 110 King Street, Manly Vale, NSW 2093, Australia

[d] School of Geography, Earth and Environmental Sciences, University of Birmingham, Edgbaston, Birmingham, B15 2TT, UK

[e] Australian Nuclear Science and Technology Organisation, Lucas Heights NSW 2234, Australia

* Corresponding author. Tel.: +612 8071 9864

E-mail address: h.rutlidge@unsw.edu.au

Abstract

Cathedral Cave, Wellington, Australia, is a natural laboratory for studying water movement and geochemical processes in the unsaturated zone by using artificial irrigation to activate drip sites within the cave. Water sampled from two drip sites activated by irrigations carried out in summer 2014 was analysed for dissolved inorganic ions and fluorescent organic matter. The analysis allowed the development of a conceptual flow path model for each drip site. DOM analysis was further complemented by liquid chromatography with organic carbon detection (LC-OCD), applied for the first time to karst drip waters, allowing the characterisation of six organic matter fractions. The differences in organic matter fractions at each drip site are interpreted as a signature of the proposed flow paths. LC-OCD was also compared with parallel factor analysis (PARAFAC) of the fluorescence and good correlations were observed for high molecular weight organic matter. Strong positive correlations were also observed for high molecular weight matter and Cu and Ni. This is suggestive of colloidal transport of Cu and Ni by organic matter with high molecular weight, while small molecular weight colloids were not efficient transporters. LC-OCD uniquely provides information on

non-fluorescent organic matter and can be used to further quantify drip water organic matter composition.

1. Introduction

There has been increasing interest in dissolved organic matter (DOM) in cave drip water and the potential use of organic markers in speleothems as paleoclimate proxies (Blyth et al., 2008; Fairchild and Baker, 2012). While initial studies focussed on bulk organic matter (Baker et al., 1997), subsequent investigations have focussed on the potential of lipid biomarkers (Xie et al., 2003; Blyth et al., 2007; Rushdi et al., 2011), polycyclic aromatic hydrocarbons (PAHs) (Perrette et al., 2013), $\delta^{13}C$ of organic matter (Blyth et al., 2013a, b) and trace elements associated with organic colloids (Hartland et al., 2012; 2014). Lipids such as n-alkanes have been shown to record vegetation and land-use change (Blyth et al., 2007; 2011) and glycerol dialkyl glycerol tetraethers have shown potential as a paleotemperature proxy (Blyth and Schouten, 2013; Blyth et al., 2014).

Cave-based monitoring programs are typically utilised to understand the processes affecting organic matter concentration and character as it is transported from the soil to the cave. Typically cave drip water organic carbon concentrations are less than 3 mg/L (Baker et al., 1997; Ban et al., 2008), and are likely to be more variable than groundwater (Shen et al., 2014). This combined with relatively small water sample volumes that can be obtained from stalagmite drip water means that unfeasibly large water sample volumes are required for most biomolecular characterisation techniques. Apart from one study on drip water PAHs (Perrette et al 2013) and one on LMW fatty acids (Bosle et al 2014), published drip water organic matter monitoring has focussed on the measurement of the fluorescent organic matter fraction (fDOM), as this requires about 4 mL of water sample, no pretreatment and has low detection limits (Baker et al., 1997; Baker and Genty, 1999), however, this technique can only provide information about the fluorescent fraction of the organic matter.

Liquid chromatography-organic carbon detection (LC-OCD) can be used to identify classes of organic compounds in water samples. It gives quantitative information on natural organic matter (NOM) and qualitative results regarding molecular size distribution of organic impurities in water. The qualitative analysis is based on size exclusion chromatography where large molecules have different degrees of interaction with the pores on the column material resulting in different retention times for different molecular size fractions.

Quantification is completed by carbon mass determination, similar to total organic carbon (TOC) analysis, performed with both UV and organic carbon IR detectors which enable DOC quantification at the sub-ppm level with only small sample volumes (10 mL). The resulting chromatograms have significantly overlapping peaks, which typically require manual processing to obtain correct peak separation, and therefore the expert knowledge of the user is important for reliable results. The technique is relatively new but has seen extensive use characterising the efficiency of water treatment processes (Zheng et al., 2010; Li et al., 2012) as well as natural organic matter (NOM) in fresh and marine waters (Velten et al., 2011; Rachman et al., 2014).

The DOC comprises hydrophobic organic carbon (HOC) that has a strong hydrophobic interaction with the column material and does not elute through the column and chromatographic dissolved organic carbon (CDOC). The HOC is determined by difference between total organic carbon, determined by bypass of the column, and the CDOC. The five different groups of CDOC that can be fractionated by the column are biopolymers, humic substances, building blocks, low molecular weight (LMW) acids and neutrals, details of these fractions are given in Table 1. These compounds are characterized by a UV-detector (λ = 254 nm) and quantified by IR-detection after UV oxidation in a cylindrical UV thin-film reactor (Huber et al., 2011).

The purpose of this study is to evaluate and compare LC-OCD and fluorescence analyses as a tool for characterisation of DOM in cave drip waters, and to understand the time evolution of organic matter fractions in the context of the routing of water between surface and drip site.

2. Material and methods

2.1 Study site

Cathedral Cave at Wellington Caves, NSW, Australia (32 37'S; 148 56'E) was used as the location for this study (Figure 1). The geology of the region has previously been described (Johnson, 1975) and the cave is within an area of massive Devonian limestone, with a thin-layer of red-brown soil comprising clays, iron oxides, fine quartz sands, and calcite nodules (Frank, 1971), with aeolian contributions (Hesse and McTanish, 2003). The site is within a temperate semi-arid region, with mean annual precipitation of 619 mm (1956-2005) and evaporation of 1825 mm (1956-2005) recorded at the nearby Wellington Research Centre

(Australia Bureau of Meteorology). There is a significant seasonal temperature variation with monthly mean maximum ranging from 15 °C in July and 32 °C in January (1956-1990, Australia Bureau of Meteorology).

The cave continues to be a focus of long-term hydrogeological monitoring (concurrent to this study) by the investigators, commencing in 2010 and continuing, primarily using a network of in-situ Stalagmate © drip loggers. Jex et al. (2012) described infiltration patterns and processes within the cave, and identified that infiltration only occurs after high magnitude and long duration rainfall events, with a total precipitation of over ~60 mm within 24-48 hours, however the necessary amount of rainfall needed can vary dependant on antecedent soil conditions. Such rainfall events occur very infrequently, typically 0-2 times a year, and require slow-moving weather systems. In winter, this is most likely associated with westerly frontal rainfall, where the associated low pressure system is slow moving, deep, and relatively close to the site. In summer, atmospheric instability and associated convective rainfall caused by slow moving or stationary troughs and associated upper level systems, draws moist, unstable air from the north of the region. Drip water isotope monitoring demonstrated that drip water $\delta^{18}O$ is dominated by epikarst evaporation (Cuthbert et al., 2014a). Due to the infrequent recharge events, evaporation from near-surface karst water stores leads to increasingly enriched cave drip waters.

Most recently, Cathedral Cave has been utilised for regular artificial irrigation experiments, to better understand karst hydrogeochemical processes. An irrigation in the summer of 2013 has been used to understand drip water trace element and organic matter hydrogeochemical evolution during recharge events (Rutlidge et al., 2014). An irrigation in the summer of 2014 has been used to understand the role of within-cave evaporation during recharge events, and identified the role of evaporative cooling on drip waters for the first time (Cuthbert et al., 2014b). Data from both irrigation experiments has been used to quantify the processes of heat transport (Rau et al., 2015). The data presented here is from water samples collected during the summer 2014 irrigation event.

2.2 Irrigation experiment

For this study, an area of approximately 5 × 10 m, directly above the study area in Cathedral Cave was irrigated with Wellington town supply water. The experiment was performed at the

height of the Australian summer and the antecedent soil moisture was low (initial average soil moisture was measured as 14.4 wt%). Two irrigations by hand hosing were performed on consecutive mornings. The irrigation on Day 1 started at 7:50 am and continued for three hours until dripping was initiated in the cave at five sites below the irrigation zone, one of which had been used for drip water sampling previously and designated Site 1 (Rutlidge et al., 2014) (Figure 1). A total of 3400 L was applied. The irrigation on Day 2 comprised two batches of irrigation water. The initial batch was 1000 L town water loaded into a tank on site and spiked with 0.5 L of 99.8% deuterium (D_2O), resulting in a deuterium enrichment of 6700 ‰ (VSMOW) as measured by laser cavity ring down mass spectrometry (see below). This batch was hand hosed for 1 ¾ hours then followed by a second non-enriched batch of 1430 L of town water for 1 ½ hours. Following this irrigation, an additional site activated and was designated Site 25 (Figure 1). Site 1 was equipped with a Stalagmate® drip logger during the experiment.

2.3 Sampling and in-cave measurements

For each drip water sample collected from Sites 1 and 25, a volume of 200-300 mL was collected, which took approximately 30 minutes. Alkalinity, pH, electrical conductivity (EC) and temperature were measured immediately after sampling. Alkalinity was determined on a 10 mL sub-sample using Gran titration with a 0.16 N H_2SO_4. Sub-samples for cation, anion, fluorescence, LC-OCD and isotopic analysis were filtered (0.45 μm) and prepared for subsequent laboratory testing, with the cation samples acidified with 2% 10 N nitric acid to ensure stability during storage. In addition, one sample from each batch of irrigation water (i.e. Day 1, Day 2 deuterium enriched and non-enriched town water) was collected for analysis as above.

2.4 Trace element and anion analysis

Trace-element analysis of the drip water and each batch of irrigation water (without dilution) was carried out using a Perkin Elmer NexION 300D ICP-MS and Perkin Elmer Optima 7300 ICP-OES. The following elements were analysed by ICP-OES: Ca, K, Mg, Na, Si and Sr, and by ICP-MS: Al, Ba, Cu, Fe, Mn, Ni and Zn (Table EA1). The method has been described in detail previously (Rutlidge et al., 2014). In addition, a Dionex Ion chromatography system was used to determine the concentration of the following anions, fluoride, chloride, nitrite, bromine, nitrate, phosphate and sulfate. Of these only chloride, bromide and sulfate were

above the detection limit (Table EA2). PHREEQC for Windows (Parkhurst & Appelo, 2003) was used to calculate saturation indices on selected minerals from the dissolved concentrations.

2.5 Fluorescence analysis

Fluorescence excitation-emission matrices (EEM's) were obtained for the collected drip water samples using a Horiba Aqualog fluorescence spectrometer. This spectrometer allows for the collection of absorbance and fluorescence within the same instrument, with the absorbance data used to correct for any reabsorption (or inner-filter) effects. Fluorescence EEMs were collected using an excitation range of 240 to 400 nm, with a step-size of 3 nm, and emitted fluorescence detected between 210 and 600 nm with a CCD detector, at a spectral resolution of 1.64 nm and integration time of 1 s. All data was inner-filter corrected, scatter lines masked, and Raman normalised (to a mean Raman intensity of water in a sealed water cell, excited at 380 nm, of 200 intensity units), using proprietary Aqualog software. The resultant dataset of 19 EEMs was analysed using a previous calibrated parallel factor analysis (PARAFAC) model for this site (see Rutlidge et al., 2014) using Eigenvector Research Solo © software. These three factors were characterised, following Ishii and Boyer (2012), as unprocessed, soil-derived humic-like and fulvic-like material (Factor 1), biogeochemically processed humic/fulvic-like material (Factor 2), and living or dead microbial matter (tryptophan-like fluorescence) (Factor 3) which is indicative of microbiological activity (Hudson et al., 2007).

2.6 LC-OCD analysis

The LC-OCD is an automated size-exclusion chromatography system coupled to three detectors, for organic carbon, organic nitrogen and UV absorbance, respectively. Details of the measurement procedure have been described in full by Huber et al. (2011). In this study, a Toyopearl TSK HW50S column was used with a phosphate buffer mobile phase of pH 6.4 at a flow rate of 1.1 mL/min. Injection volumes were 1 mL. The chromatographic column is a weak cation exchange column containing a polymethacrylate filter. The chromatography subdivides into six sub-fractions, which are assigned to specific classes of compounds: that is biopolymers, humics, building blocks, low molecular-weight neutrals and hydrophobic organic carbon (Huber et al., 2011).

2.7 Deuterium analysis

The isotopic composition of irrigation and drip water samples were determined using an LGR-100DT V2 off-axis, integrated cavity output, cavity ring-down mass-spectrometer (Wassenaar et al., 2008; Cuthbert et al., 2014a) at UNSW Australia. Each sample was run with a total of 10 injections and run in triplicate (total of 30 injections), with the average of the replicates used as the reported value. Four internal reference standards provided by the Australian Nuclear Science and Technology Organisation with deuterium values of: -174.1, -78.8, -6.54, 32.3 ‰ VSMOW were used. An additional independent laboratory reference standard was used from Elemental Microanalysis with deuterium value of 4.93 relative to VSMOW. The analytical precision for deuterium were ~1.5‰ VSMOW (1σ; calculated from within run internal reference materials). This compares to an external precision for deuterium of 0.6‰ (1σ, analysis of standards). The calibration curve was calculated using the reference standards and was used to interpolate drip water and irrigation water samples. Samples which fell outside of the range of the reference standards were extrapolated.

3. Results

Figure 2 shows the drip rate data for Site 1 over the course of the experiment. Dripping at Site 1 activated on Day 1 and stopped on Day 3, while a secondary site, Site 25, activated on Day 2 and continued on Day 3 and beyond. At Site 1, the two irrigations above the cave resulted in two significant pulses, with a three hour delay on Day 1 and one hour delay on Day 2 from the start of each irrigation. The second site considered in this study (Site 25) was an unexpected activation on Day 2 in a relatively inaccessible location in the cave and no measured drip rate data is available, however sampling for both sites was possible over the course of the experiment allowing both sites to be chemically characterised. When dripping had commenced at Site 25 it was observed to be consistent but at a lower frequency than the initial activation at Site 1, suggesting there are flow restrictions at this site relative to Site 1. Site 1 shows an overall higher pH, lower alkalinity and Ca concentration than Site 25. This is reflected in the PHREEQC calculated PCO_2 and saturation indices for calcite that are both lower for Site 1. Calculations indicate near saturation of calcite at Site 25 and a PCO_2 that is an order of magnitude higher than at Site 1.

A previous study by the authors at this location established that certain elements were derived predominantly from either the bedrock or the soil using a principal component analysis (PCA) model (Rutlidge et al., 2014). Ba, Cu and Ni were soil-derived elements and Ca and Sr were limestone bedrock-derived elements. A soil source for both Ni and Cu is likely as they

are both organo-colloid associated trace elements (Hartland et al., 2012). Ba was not detected in limestone bedrock samples and since it is strongly absorbed to clay minerals, the clay-rich soils likely provide the dominant source of the Ba. Table 2 shows that at Site 1 the bedrock-derived Ca concentration was lower than at Site 25, while the soil-derived elements of Ba, Cu and Ni were higher. A relatively small difference was observed for Sr between the two sites. While the initial concentrations of elements in irrigation water were comparable to the drip water concentrations, irrigation water does not make a significant contribution to the measured drip water concentrations due to dilution with existing stored water, based on the deuterium measurements (see Table 2). A minimum dilution down to 3.5% can be estimated based on the initial deuterium isotope ratio in the irrigation tank (6700‰ VSMOW) and the maximum deuterium ratio measured at Site 1 of 220‰ VSMOW against the background deuterium ratio of -13‰ VSMOW. The deuterium ratio measured at Site 25 (38‰ VSMOW on average) is above the background level (assumed to be same as Site 1) but relatively consistent and significantly lower than the maximum value for Site 1.

Figure 3 shows the behaviour of the PARAFAC factors derived from the analysis of the fluorescent EEM data over the course of the study. The three factors characterised were unprocessed, soil-derived humic-like and fulvic-like material (Factor 1), biogeochemically processed humic/fulvic-like material (Factor 2), and living or dead microbial matter (tryptophan-like fluorescence) (Factor 3). These three factors are the same as those observed in the 2013 irrigation experiments (Rutlidge et al., 2013). Overall the drip water from Site 1 contains more organic matter than Site 25. Factor 1 and Factor 2 show a relatively small decrease between the two irrigations at Site 1. At Site 25 these factors are relatively constant. Factor 3 (microbial-derived) shows initial high values for the first irrigation and then decreasing for the second irrigation at Site 1 compared to Site 25 where it is relatively unchanged.

Figure 4 shows the time-series concentration profiles for the organic fractions measured by LC-OCD for both sites. Overall the DOC concentration at Site 1, as measured by LC-OCD, decreased over the course of the study, while at Site 25 the DOC concentration was lower and remained relatively unchanged. The DOC fraction comprises both HOC (hydrophobic) and CDOC (hydrophilic) organic carbon. The CDOC fraction can be further broken down into

chemical fractions of bio-polymers, humics, building blocks and LMW neutrals. For both sites the concentration of CDOC (Site 1 average was 4565 µg/L and Site 25 average was 2150 µg/L) was significantly higher than the HOC concentrations (the average values for Site 1 and Site 25 were 1213 µg/L and 736 µg/L respectively). In terms of individual fractions, the bio-polymers decreased over time at Site 1 but were close to the detection limit at Site 25. Building blocks were fairly consistent each day but showed a decrease from day to day at Site 1.

Table EA3 shows the Kendall tau correlations between selected elements and the LC-OCD fractions. Ca (bedrock-derived) shows negative correlations with DOC (-0.61), CDOC (-0.61) and humics (-0.66). While Cu and Ni (soil-derived) show positive correlations with all LC-OCD fractions except building blocks and LMW neutrals. Ba shows positive correlations with DOC (0.62) and humics (0.62).

Overall the irrigation water contains the highest proportion of CDOC (hydrophilic) followed by Site 1, with Site 25 the lowest. Conversely, HOC (hydrophobic) showed the lowest proportion in the irrigation water, increasing in Site 1 and again in Site 25. There are clear differences in the relative proportions of the different hydrophilic fractions measured by LC-OCD in the DOC of the irrigation water and the drip water from the two sites as shown in Figure 5. Site 1 has higher proportion of humics, building blocks & bio-polymers while Site 25 has a higher proportion of LMW neutrals. Site 25 shows the most difference from the irrigation water.

4. Discussion

4.1 Flow path Model

After the first irrigation dripping at Site 1 responded within 3 hours, with an initial high drip rate decreasing over 20 hours. This ‘flashy’ flow response, in combination with a short arrival time for the deuterium tracer, suggests a short flow path for Site 1. This is supported by an excavation that revealed a soil filled void in the limestone directly above Site 1, and a measured maximum bedrock thickness of only ~ 1.5 m. In comparison, Site 25 showed a lagged and damped flow response and deuterium tracer breakthrough, suggesting a combination of more unsaturated zone storage water, tortuous/longer pathways through the epikarst and lower fracture permeability. Deuterium measurements at both sites showed significant dilution by existing stores of water. Site 25 showed a higher level of dilution of

304 the tracer (down to 0.9%) compared to Site 1 (down to 3.5%), suggesting that the Site 25
305 store contained more water. This increased dilution can partly explain the decreased total
306 DOC observed at Site 25 compared to Site 1.
307
308 Since cave drip water carries a chemical signature indicative of its flow path, the analysis
309 provided here can be used to reveal characteristics of flow routing between surface and cave.
310 Our interpretation benefits from the long-term drip water isotope monitoring program at the
311 cave (Cuthbert et al 2014a). That study demonstrated the ubiquitous presence of enriched drip
312 water isotopes, that could only be explained by evaporation from water stored in fractures or
313 voids the shallow vadose zone. Site 1 has PCO_2 values (Figure 2) only slightly elevated
314 above atmospheric values that could indicate poor CO_2 production in the soil, loss of
315 produced CO_2 by ventilation, or degassing as the water flowed down over the exposed
316 flowstone surface between the exfiltration point and drip site. Site 25 on the other hand had
317 PCO_2 values about one order of magnitude above those of Site 1 due to longer residence
318 times in the bedrock and a more restricted pore space minimising CO_2 loss to the atmosphere.
319 The recorded pH values largely reflect the calculated PCO_2 values, but may be tempered by
320 calcite dissolution (hence the near neutral pH values). Calcium, alkalinity and the saturation
321 index (SI) for calcite indicate that water sampled at Site 25 is more 'evolved' since it is closer
322 to equilibrium with calcite. It further indicates that there was a larger volume of stored water
323 in the flow path connecting to Site 25. Conversely at Site 1, the inorganic carbon
324 observations suggest that there is lower volume of stored water and that the store is in the soil
325 above the limestone. This is supported by higher concentrations of trace elements at Site 1
326 previously shown to be associated with soil at this study location, specifically Ba, Cu and Ni
327 (Rutlidge et al., 2014).
328
329 Figure 6 shows a proposed schematic of flow paths for Sites 1 and 25 derived from the
330 observations above. In summary, Site 1 drip water travels through a void in the bedrock that
331 was filled with partially saturated soil, followed by further passage through a relatively thin
332 (<1.5m) amount of limestone, before entering the cave near the cave roof. The water
333 continues to flow over the cave wall, forming a flowstone deposit, before dripping from a
334 stalactite at Site 1. . Site 25 is fed by a long thin bedrock fracture, or a series of fractures,
335 which requires more water to enter the epikarst and/or more time than Site 1 before activating
336 the drip point.
337

338 4.2 Correlations between PARAFAC, LC-OCD and trace elements

339 The site had experienced a total of only 88 mm of rainfall over six events in the three months
340 prior to the irrigation and as a result the volume of water required to overcome the soil
341 moisture deficit and activate dripping was at least 1500 L. This volume of water was only
342 available from the local town water supply where DOM is present at comparable levels to
343 those measured in the drip water. Hence, DOM in the drip water will be derived from existing
344 DOM in town water and DOM extracted from soil organic matter in the epikarst. However,
345 as with the trace elements the DOM in the irrigation water would be diluted by the existing
346 water stored in the epikarst.

347

348 Figure 7 shows plots of selected LC-OCD derived classes of compounds that can be related
349 to the three corresponding PARAFAC factors from all samples taken over the course of the
350 study. Factor 1, unprocessed humic and fulvic acids, shows a strong correlation with the LC-
351 OCD humic fraction (Kendall tau coefficient of 0.61), as does Factor 2 (Kendall tau
352 coefficient of 0.79), which is processed humic and fulvic acids. The LC-OCD humic fraction
353 therefore correlates with the two PARAFAC factors which are also associated with humic-
354 like material, with the PARAFAC analysis suggesting that the LC-OCD humic fraction
355 comprises two different optical components. Factor 3 shows the highest correlation with bio-
356 polymers (Kendall tau coefficient of 0.69). Factor 3 is characterised as tryptophan-like
357 fluorescence, typically derived from living or dead microbial matter, and the correlation with
358 bio-polymers suggests a microbial biopolymer source.In addition to the plots shown in Figure
359 6, Factor 1 and 2 are positively correlated with DOC measured by LC-OCD, and the HOC
360 (hydrophobic) and CDOC (hydrophilic) LC-OCD fractions (see Table EA3). Factor 1 is also
361 positively correlated with the derived aromaticity index and Factor 2 with the building block
362 fraction. In most cases the LC-OCD derived indices, aromaticity, molecular weight, inorganic
363 colloids and specific UV absorbance (SUVA) did not show strong correlations with any
364 PARAFAC factors or LC-OCD fractions. The correlations observed in Figure 7 demonstrate
365 that LC-OCD agrees with the PARAFAC factor assignments from the fluorescence analysis.

366

367 LC-OCD uniquely provides information on non-fluorescent organic matter and can be used to
368 identify and quantify changes in organic matter composition. Figure 8 shows individual
369 scatter plots of the LC-OCD fractions and HOC (hydrophobic) expressed in terms of percent
370 of total DOC, to minimise the changes due to dilution. LMW neutrals are relatively higher at
371 Site 25 than Site 1 indicating that they are highly mobile and eluted rapidly as expected for

uncharged low molecular weight DOM (Shen et al., 2014). In contrast building blocks are relatively lower at Site 25 compared to Site 1 which suggests that they are interacting with the calcite surface in the epikarst (Alipour Tabrizy et al. 2011; Suess, 1970 and Suess, 1973).

Drip water from Site 25 consistently contained low levels of biopolymer and were often below detection. Along with the correlation with PARAFAC Factor 3, this suggests that there was an initial flush of biopolymer at Site 1 that would be expected to have accumulated in the partially saturated lower soil layer prior to the first irrigation. The LC-OCD biopolymer fraction is defined as being >20 kDa and hydrophilic (Huber et al 2011) organic compounds such as polysaccharides. We hypothesise that the longer flow path at Site 25 leads to greater loss of this fraction, for example by microbial degradation, compared to Site 1.

The relative decrease in the humic substances fraction at Site 25 can be explained by the preferential adsorption of the negatively charged humic fraction at the positively charged calcite surface during flow through the bedrock fracture. We observe ongoing calcite formation in the form of active flowstone deposits (Site 1) and stalactite formation (Sites 1 and 25). Ongoing calcite formation from solution provides a continual source of fresh surfaces that are positively charged at the drip water pH (approximately 8), below the point of zero charge of calcite, pH_{PZC} = 9.5 (Appelo and Postma, 2005). This preferential adsorption is supported by numerous laboratory studies of organic matter interaction with calcite (Alipour Tabrizy et al. 2011; Suess, 1970 and Suess, 1973). LC-OCD therefore helps identify changes in organic matter composition, with loss of different organic matter fractions due to processes which include sorption and microbial processing. Such changes in composition can be conceived as a smaller-scale manifestation of the "regional scale chromatography" proposed for groundwater (Hedges et al., 1986; Shen et al., 2014).

Strong positive correlations were observed for Cu and Ni with the higher molecular weight LC-OCD fractions, for example biopolymers-Cu (0.76) and humics-Ni (0.80). This supports a prior study by Hartland et al (2012) who used flow field-flow fractionation of karst drip waters that showed colloidal transport of Cu and Ni by organic matter with high molecular weight. This same study observed that small molecular weight colloids were not efficient transporters of Cu and Ni, and we further confirm this observation here as we see low correlations observed for these elements and the LMW neutrals (0.40 and 0.24, respectively). We also considered the relationship between the Cu/Ni ratio and LC-OCD fractions and

derived indices (Table EA3 and Figure 9). Hartland et al (2012) have previously hypothesised that the Cu/Ni ratio in cave drip waters is indicative of a quality change in DOM, as Cu has an increased affinity to binding to aromatic binding sites than Ni. For the whole dataset (Table EA2), our results show that the only statistically significant correlation between Cu/Ni and LC-OCD fractions is a negative correlation with humics (-0.49) and we see no significant correlations between Cu/Ni and the derived indices of molecular weight or aromaticity. However, at a site-by-site basis (Figure 9), we observe that these global correlations are masking site-specific patterns. At Site 1, there are positive correlations between Cu/Ni and aromaticity and molecular weight, as predicted by Hartland et al (2012), and also with building blocks and LMW neutrals. In contrast, correlations between Cu/Ni and LC-OCD fractions and derived indices are very weak at Site 25, but the site as a whole has high Cu/Ni than Site 1, which explains the global negative correlations observed (Table EA2). Our LC-OCD results suggest a complex relationship between organic matter character as determined by LC-OCD and Cu/Ni over the event timescale which requires further investigation.

Compared with fluorescence analysis LC-OCD provides more information on the types of colloid-forming DOM involved in metal transport. Our results that demonstrate correlation between Cu and Ni concentration and DOM concentration for all data, but only with the largest size fractions (humics and biopolymers). The correlation between Cu/Ni and aromaticity varies between the two sites. It is strongest at Site 1, despite the lack of correlation between humic fraction concentration and Cu/Ni, confirming an aromaticity control on Cu/Ni (Hartland et al. 2012). However, variations in the correlation with LC-OCD fractions and indices between flow paths and within recharge events suggest that flow switching and discharge variability may be preserved in speleothem records of these organic-transported metals.

5. Conclusions

Trace element composition measured by ICP and organic matter analysis by fluorescence has been applied to cave drip water samples collected after a series of artificial irrigations. This revealed an understanding of the flow paths feeding two drip sites. We propose that Site 1 is fed by a short and permeable bedrock fracture via a soil store which retains relatively high moisture content during periods of no rainfall. In comparison the data suggest that Site 25 is fed by an area of thinner, drier soil through a thicker epikarst with greater unsaturated storage and/or lower permeability.

DOM analysis was also performed by LC-OCD, applied for the first time to karst drip waters. Good correlations were observed between LC-OCD humic and bio-polymer fractions and the corresponding PARAFAC factors from the fluorescent analysis. LC-OCD enabled a more detailed characterisation of the non-fluorescent fractions of DOM present in the drip water sample. LC-OCD identified that as the drip water moves through bedrock fractures there are changes in dissolved organic matter composition which will depend on the path-length of the water. Locations nearer the surface with shorter path-length and higher discharge have higher DOC, as there is less time for organic matter sorption and microbial processing. At Site 25, with the longer path-length, this leads to the preferential adsorption of the humic substance fraction, resulting in a relative decease in the hydrophilic portion of DOM compared to Site 1, while the uncharged low molecular weight neutrals pass through unaffected.

LC-OCD provides insights into vadose zone processes affecting dissolved organic matter, such as sorption and microbial processing, which occur between different flow paths, within discharge events and between discharge events. The greater level of chemical detail, unique to LC-OCD, demonstrates its potential for providing insight into the evolution of organic matter from soil to cave, through different flow paths in the unsaturated zone. An improved understanding of these processes could have implications for selecting speleothem samples suitable for biomarker research, such as when using lipids for paleoclimate reconstructions (Blyth et al., 2007) or fluorescent organic matter to construct fluorescence lamina growth chronologies (Baker et al., 1993). Research presented here, focusing on just two drip waters of contrasting flow path-length, needs to be extended for a wider range of drip sites and caves using LC-OCD.

5. Acknowledgements

We thank the staff at Wellington Caves for their support. Funding for this research was provided by the National Centre for Groundwater Research and Training, an Australian Government initiative, supported by the Australian Research Council and the National Water Commission and Mark Wainwright Analytical Centre at UNSW Australia. Mark Cuthbert was supported by Marie Curie Research Fellowship funding from the European Community's Seventh Framework Programme [FP7/2007-2013] under grant agreement n°299091. We also acknowledge the anonymous reviewers that provided helpful feedback.

6. References

Alipour Tabrizy, V., Denoyel, R. and Hamouda, A.A. (2011). Characterization of wettability alteration of calcite, quartz and kaolinite: Surface energy analysis. *Colloids and Surfaces A: Physicochemical and Engineering Aspects* **384**, 98-108.

Appelo, C.A.J. and Postma, D. (2005). *Geochemistry, Groundwater, and Pollution*, second ed. A.A. Balkema, Rotterdam, 649 pp.

Baker, A., Smart, P. L., Edwards, R. L., and Richards, D. A. (1993). Annual growth banding in a cave stalagmite. *Nature*, **364**, 518-520.

Baker, A., Barnes, W.L. and Smart, P.L. (1997). Stalagmite Drip Discharge and Organic Matter Fluxes in Lower Cave, Bristol. *Hydrological Processes* **11**, 1541-1555.

Baker, A. and Genty, D. (1999). Fluorescence wavelength and intensity variations of cave waters. *Journal of Hydrology* **217**, 19-34.

Ban, F., Pan, G., Zhu, J., Cai, B., and Tan, M. (2008). Temporal and spatial variations in the discharge and dissolved organic carbon of drip waters in Beijing Shihua Cave, China. *Hydrological Processes* **22**, 3749-3758.

Blyth, A.J., Asrat, A., Baker, A., Gulliver, P., Leng, M.J. and Genty, D. (2007). A new approach to detecting vegetation and land-use change using high-resolution lipid biomarker records in stalagmites. *Quaternary Research* **68**, 314-324.

Blyth, A.J., Baker, A., Collins, M.J., Penkman, K.E.H., Gilmour, M.A., Moss, J.S., Genty, D. and Drysdale, R.N. (2008). Molecular organic matter in speleothems and its potential as an environmental proxy. *Quaternary Science Reviews* **27**, 905-921.

Blyth, A.J., Thomas, L.E., Calsteren, P.V. and Baker, A. (2011). A 2000 year lipid biomarker record preserved in a stalagmite from NW Scotland. *Journal of Quaternary Science* **26**, 326-334.

Blyth, A.J., Shutova, Y. and Smith, C.I. (2013). $\delta^{13}C$ analysis of bulk organic matter in speleothems using liquid chromatography–isotope ratio mass spectrometry. *Organic Geochemistry* **55**, 22-25.

Blyth, A.J., Smith, C.I. and Drysdale, R.N. (2013). A new perspective on the $\delta^{13}C$ signal preserved in speleothems using LC-IRMS analysis of bulk organic matter and compound specific stable isotope analysis. *Quaternary Science Reviews* **75**, 143-149.

Blyth, A.J. and Schouten, S. (2013). Calibrating the glycerol dialkyl glycerol tetraether temperature signal in speleothems. *Geochimica Cosmochimica Acta* **109**, 312-328.

Blyth, A.J., Jex, C., Baker, A., Khan, S.J. and Schouten, S. (2014). Contrasting distributions of glycerol dialkyl glycerol tetraethers (GDGTs) in speleothems and associated soils. *Organic Geochemistry* **69**, 1-10.

Bosle, J.M., Mischel, S.A., Schulze A.-L., Scholz, D. and Hoffman, T. (2014) Quantification of low molecular weight fatty acids in cave drip water and speleothems using HPLC-ESI-IT/MS – development and validation of a selectiv emethod. *Anal. Bioanal. Chem.*, **406**, 3167-3177.

Cuthbert, M.O., Baker, A., Jex, C.N., Graham, P.W., Treble, P.C., Andersen, M.S. and Acworth, R.I. (2014a). Drip water isotopes in semi-arid karst: Implications for speleothem paleoclimatology, *Earth and Planetary Science Letters* **395**, 194-204.

Cuthbert, M.O., Rau, G.C., Andersen, M.S., Roshan, H., Rutlidge, H., Marjo, C.E., Markowska, M., Jex, C.N., Graham, P.W., Mariethoz, G. Acworth, R.I. and Baker, A. (2014b). Evaporative cooling of speleothem drip water. *Scientific Reports* **4**, .

Fairchild I. J. and Baker A. (2012) *Speleothem Science*. Wiley-Blackwell, 432 pp.

Frank, R. (1971). The clastic sediments of the Wellington Caves, New South Wales. *Helictite* **9**, 3-26.

Hartland, A., Fairchild, I.J., Lead, J.R., Borsato, A., Baker, A., Frisia, S. and Baalousha, M. (2012). From soil to cave: transport of trace metals by natural organic matter in cave dripwaters. *Chemical Geology* **304-305**, 68-82.

Hartland, A., Fairchild, I.J., Müller, W. and Dominguez-Villar, D. (2014). Preservation of NOM-metal complexes in a modern hyperalkaline stalagmite: Implications for speleothem trace element geochemistry. *Geochimica et Cosmochimica Acta* **128**, 29-43.

Hedges, J.I., Ertel, J.L., Quay, P.D., Grootes, P.M., Richey, J.E., Devol A.H., Farewell G.W., Schmidt, F.W., and Salati, E. (1986). Organic carbon-14 in the Amazon River system. *Science* **231**, 1129-1131.

Hesse P.P. and McTanish, G.H. (2003). Australian dust deposits: modern processes and the Quaternary record. *Quaternary Sciences Reviews* **22**, 2007-2035.

Huber, S.A., Balz, A., Abert, M. and Pronk, W. (2011). Characterisation of aquatic humic and non-humic matter with size-exclusion chromatography – organic carbon detection – organic nitrogen detection (LC-OCD-OND). *Water Research* **45**, 879-885.

Hudson, N., Baker, A., Ward, D., Reynolds, D.M., Brunsdon, C., Carliell-Marquet, C. and Browning, S. (2008). Can fluorescence spectrometry be used as a surrogate for the Biochemical Oxygen Demand (BOD) test in water quality assessment? An example from South West England. *Science of the Total Environment* **391**, 149-158.

Ishii S. K. and Boyer T. H. (2012). Behavior of reoccurring PARAFAC components in fluorescent dissolved organic matter in natural and engineered systems: A critical review. *Environmental Science and Technology* **46**, 2006–2017.

Jex C. N., Mariethoz G., Baker A., Graham P., Andersen M. S., Acworth I., Edwards N. and Azcurra C. (2012). Spatially dense drip hydrological monitoring and infiltration behaviour at the Wellington Caves, South East Australia. *International Journal of Speleology*. **41**, 285–298.

Johnson, B.D. (1975). The Garra Formation (early Devonian) at Wellington, N.S.W. *Journal and Proceedings of The Royal Society of New South Wales* **108**, 111-118.

Li, S., Heijman, S.G.J., Verberk, J.Q.J.C., Verliefde, A.R.D., Amy, G.L. and van Dijk, J.C. (2012). Removal of different fractions of NOM foulants during demineralized water backwashing. *Separation and Purification Technology* **98**, 186-192.

Parkhurst, D. L. and Appelo C. A. J. (2003). PHREEQC for Windows: A Computer Program for Speciation, Batch-Reaction, One-Dimensional Transport, and Inverse Geochemical Calculations;[2.8. 03]. USGC, Washington, DC.

Perrette, Y., Poulenard, J., Durand, A., quiers, M., Malet, E., Fanget, B and Naffrechoux E. (2013) Atmopsheric sources and soil filtering of PAH content in karst seepage waters. *Organic Geochemistry* **65**, 37-45

Rachman, R.M., Li, S., Missimer, T.M. (2014). SWRO feed water quality improvement using subsurface intakes in Oman, Spain, Turks and Caicos Islands, and Saudi Arabia. *Desalination*, **351**, 88-100.

Rau, G.C., Cuthbert , M.O., Andersen, M.S., Baker, A., Rutlidge, H., Markowska, M., Roshan, H., Marjo, C.E., Graham, P.W. and Acworth, R.I (2015). Controls on cave drip water temperature and implications for speleothem based paleoclimate reconstructions. *Quaternary Science Reviews*, in press.

Rushdi, A.I., Clark, P.U., Mix, A.C., Ersek ,V., Simoneit, B.R.T., Cheng, H. and Edwards, R.L. (2011). Composition and sources of lipid compounds in speleothem calcite from southwestern Oregon and their paleoenvironmental implications. *Environmental Earth Sciences* **62**, 1245-1261.

Rutlidge, H., Baker, A., Marjo, C.E., Andersen, M.S., Graham, P.W., Cuthbert, M.O., Rau, G.C., Roshan, H., Markowska, M., Mariethoz, G. and Jex, C.N. (2014). Dripwater organic matter and trace element geochemistry in a semi-arid karst environment: Implications for speleothem paleoclimatology. *Geochimica et Cosmochimica Acta* **135**, 217-230.

573 Shen, Y., Chapelle, F.H., Strom, E.W., and Benner R. (2014). Origins and bioavailablity of
574 dissolved organic matter in groundwater. *Biogeochemistry* DOI 10.1007/s10533-014-
575 0029-4.
576 Suess, E. (1970). Interaction of organic compounds with calcium carbonate—I. Association
577 phenomena and geochemical implications. *Geochimica et Cosmochimica Acta* **34**, 157-
578 168.
579 Suess, E. (1973). Interaction of organic compounds with calcium carbonate-II. Organo-
580 carbonate association in recent sediments. *Geochimica et Cosmochimica Acta* **37**, 2435-
581 2447.
582 Velten, S., Knappe, D.R.U., Traber, J., Kaiser, H-P., von Gunten, U., Boller, M. and Meylan,
583 S. (2011). Characterization of natural organic matter adsorption in granular activated
584 carbon adsorbers. *Water Research* **45**, 3951-3959.
585 Xie, S., Yi, Y., Huang, J., Hu, C., Cai, Y., Collins, M. and Baker A. (2003). Lipid distribution
586 in a subtropical southern China stalagmite as a record of soil ecosystem response to
587 paleoclimate change. *Quaternary Research* **60**, 340-347.
588 Zheng, X.; Ernst, M., Jekel, M. (2010). Pilot-scale investigation on the removal of organic
589 foulants in secondary effluent by slow sand filtration prior to ultrafiltration. *Water*
590 *Research* **44**, 3203-3213.
591

592 **Captions**

593 Table 1: The fractions and derived indices obtained from LC-OCD.
594

595 Table 2: Average trace element concentrations for the irrigation water and Site 1 and 25.
596 Irrigation contribution is the estimated concentration of elements from the irrigation water to
597 the cave drip water after dilution by existing water stored in the vadose zone based on
598 deuterium measurements.
599

600 Figure 1 : Plan view of the study site at Cathedral Cave, Wellington Caves (top), with a
601 boxed area indicating the surface irrigation area and cave locations of the drip sites (adapted
602 from Sydney University Speleology Society survey map 2006-2007). The study site is in the
603 state of New South Wales in south eastern Australia (bottom).
604

Figure 2: Drip rate data (Site 1 only), deuterium, pH, alkalinity, Ca, LogPCO_2 and saturation index for calcite (Sites 1 and 25) for the irrigation water and drip water samples. Grey vertical bars indicate the irrigation periods. Lines between datapoints indicate periods of continuous dripping.

Figure 3: PARAFAC factors 1-3 over time from the analysis of the fluorescence EEM data. Lines between datapoints indicate periods of continuous dripping.

Figure 4: Time series of LC-OCD fractions for both sites. Lines between datapoints indicate periods of continuous dripping.

Figure 5: Average composition of the DOC fraction for the irrigation water and both sites.

Figure 6: Simplified schematic of the different flow paths (prior to irrigation) derived from the chemical signature of the drip water. The width of markers on each axis corresponds to one metre.

Figure 7: PARAFAC factors versus selected LC-OCD fractions.

Figure 8: Matrix scatter plot of the percent of DOC of the LC-OCD fractions.

Figure 9: Matrix scatter plot of Cu/Ni against the LC-OCD fractions and indices.

606 Xie, S., Yi, Y., Huang, J., Hu, C., Cai, Y., Collins, M. and Baker A. (2003). Lipid distribution
607 in a subtropical southern China stalagmite as a record of soil ecosystem response to
608 paleoclimate change. *Quaternary Research* **60**, 340-347.
609 Zheng, X.; Ernst, M., Jekel, M. (2010). Pilot-scale investigation on the removal of organic
610 foulants in secondary effluent by slow sand filtration prior to ultrafiltration. *Water*
611 *Research* **44**, 3203-3213.
612

613 **Captions**

614 Table 1: The fractions and derived indices obtained from LC-OCD.
615

616 Table 2: Average trace element concentrations for the irrigation water and Site 1 and 25.
617 Irrigation contribution is the estimated concentration of elements from the irrigation water to
618 the cave drip water after dilution by existing water stored in the vadose zone based on
619 deuterium measurements.
620

621 Figure 1 : Plan view of the study site at Cathedral Cave, Wellington Caves (top), with a
622 boxed area indicating the surface irrigation area and cave locations of the drip sites (adapted
623 from Sydney University Speleology Society survey map 2006-2007). The study site is in the
624 state of New South Wales in south eastern Australia (bottom).
625

626 Figure 2: Drip rate data (Site 1 only), deuterium, pH, alkalinity, Ca, LogPCO_2 and saturation
627 index for calcite (Sites 1 and 25) for the irrigation water and drip water samples. Grey
628 vertical bars indicate the irrigation periods. Lines between datapoints indicate periods of
629 continuous dripping.
630

631 Figure 3: PARAFAC factors 1-3 over time from the analysis of the fluorescence EEM data.
632 Lines between datapoints indicate periods of continuous dripping.
633

634 Figure 4: Time series of LC-OCD fractions for both sites. Lines between datapoints indicate
635 periods of continuous dripping.
636

637 Figure 5: Average composition of the DOC fraction for the irrigation water and both sites.
638

Table1

		Description
Fraction	Biopolymers	Organic matter with high molecular weight, including polysaccharides, proteins and aminosugers. (Molecular weight > 20 kDa)
	Humics	Mixture of acids containing carboxyl and phenolate groups produced by biodegradation of dead organic matter. (Molecular weight ~ 1000 Da)
	Building blocks	Molecular chains of polyphenolics/polyaromatic acids that have deaggregated, due to breakage of hydrogen bonding and electrostatic interactions. (Molecular weight 300 – 500 Da)
	Low molecular weight (LMW) acids	Representing protic organic acids. (Molecular weight < 350 Da)
	Low molecular weight (LMW) neutrals	Uncharged small organics, including LMW alcohols, aldehydes, ketones, sugars and LMW amino acids. (Molecular weight < 350 Da)
	Hydrophobic organic carbon (HOC)	Fraction of DOC remaining in the column, implying a strong hydrophobic interaction with the column material, comprising longer chain aliphatic and polycyclic aromatic material.
Index	Aromaticity	Aromaticity provides an estimation of the degree of aromatic and unsaturated structures of the humic fraction.
	Molecular weight	A derived value of average molecular mass of the humic fraction.
	Inorganic colloids	Negatively charged inorganic polyelectrolytes, polyhydroxides and oxidhydrates of Fe, Al, S or Si, detected by UV light-scattering.
	SUVA	An additional parameter derived from the ratio of DOC and spectral absorption coefficient.

Table2

Table 2: Average trace element concentrations for the irrigation water and Site 1 and 25. Irrigation contribution is the estimated concentration of elements from the irrigation water to the cave drip water after dilution by existing water stored in the vadose zone based on deuterium measurements.

	Ca	Sr	Ba	Cu	Ni
	mg/L	mg/L	µg/L	µg/L	µg/L
Irrigation	26.93	0.18	59.71	1.32	0.67
Irrigation contribution	0.90	0.006	2.00	0.04	0.02
Site 1	97.68	0.07	10.77	0.90	0.26
Site 25	116.73	0.06	8.77	0.21	0.05

Figure1

Click here to download high resolution image

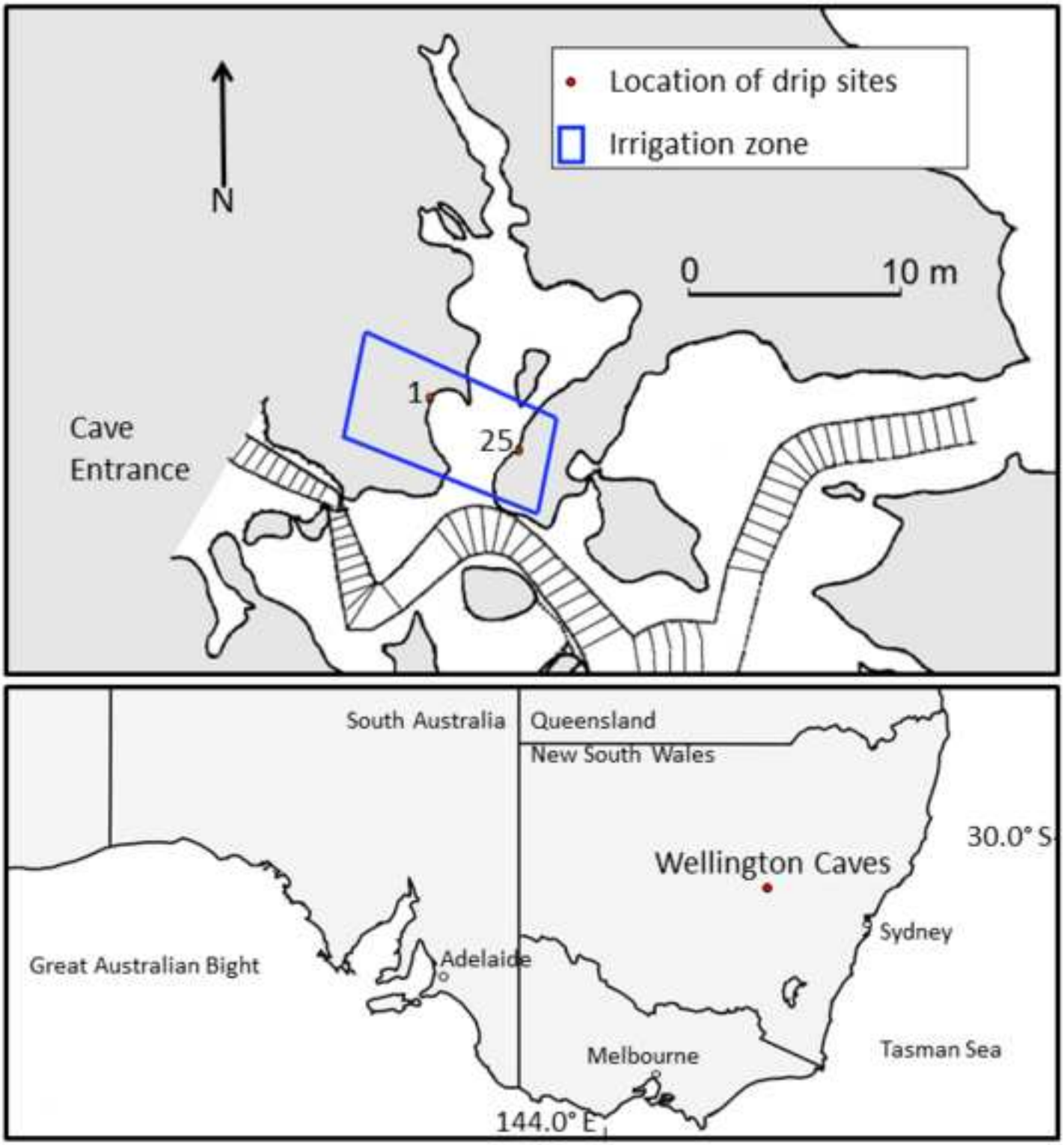

Figure2

Click here to download high resolution image

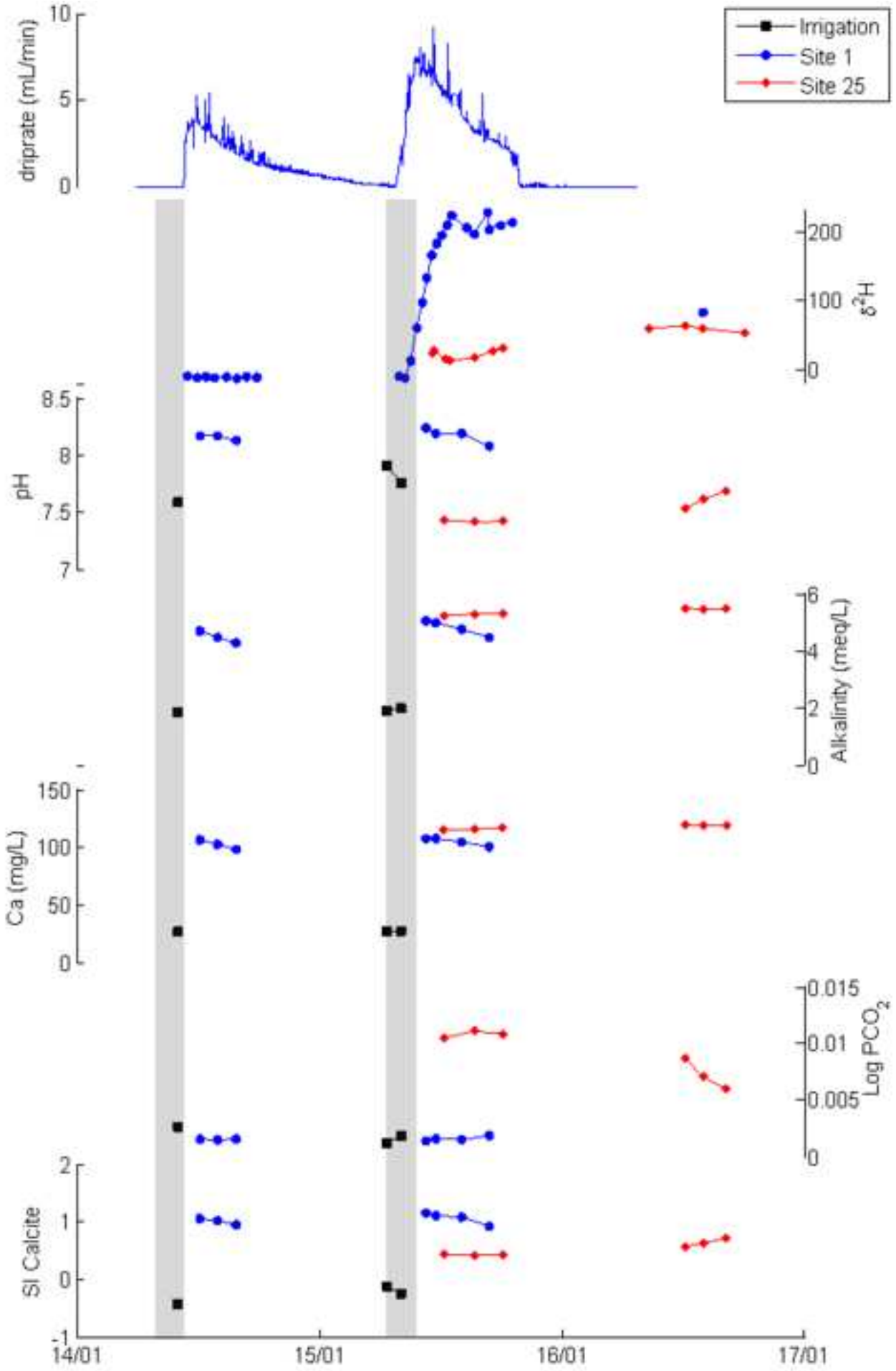

Figure3

Click here to download high resolution image

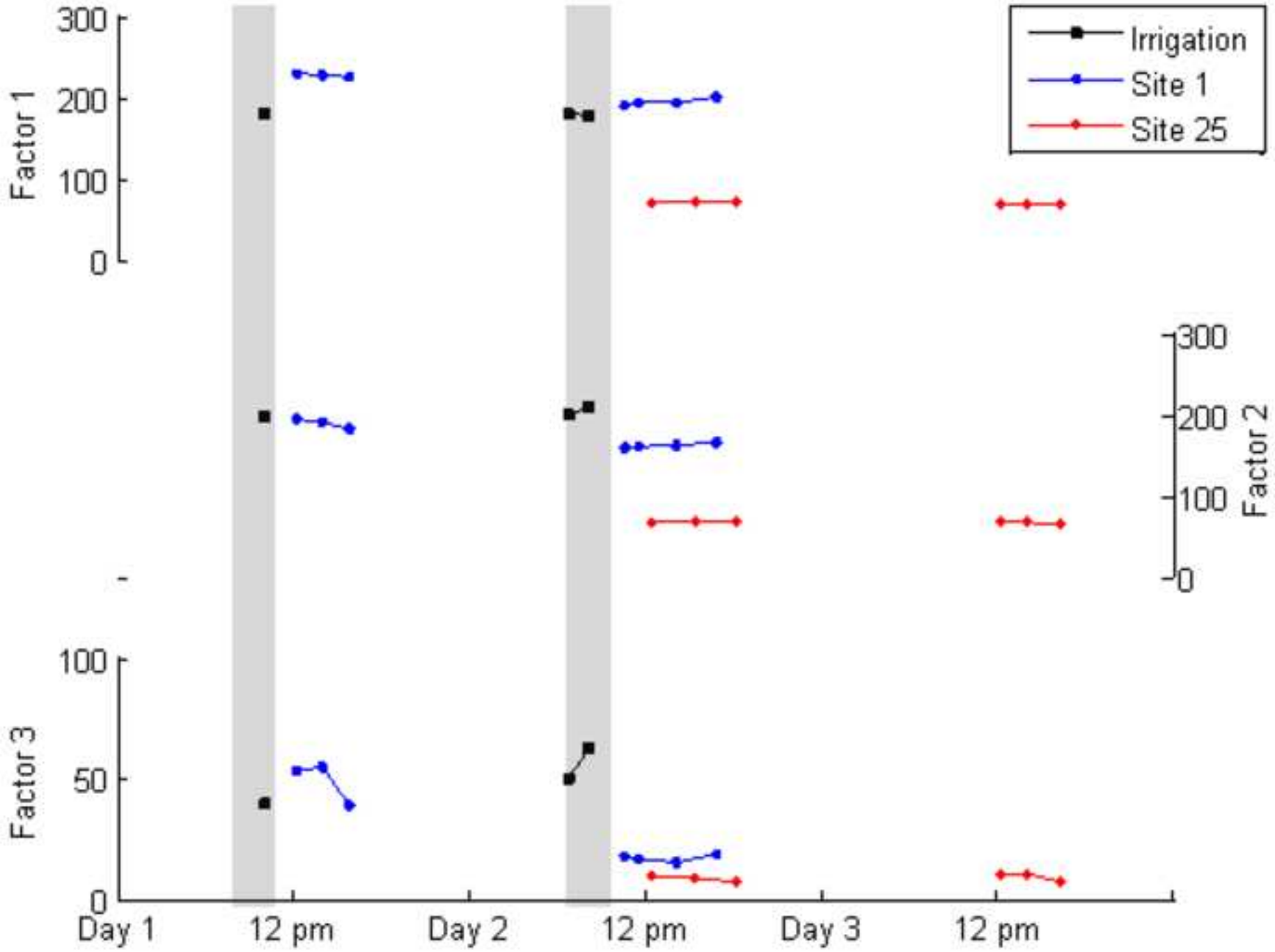

Figure4

Click here to download high resolution image

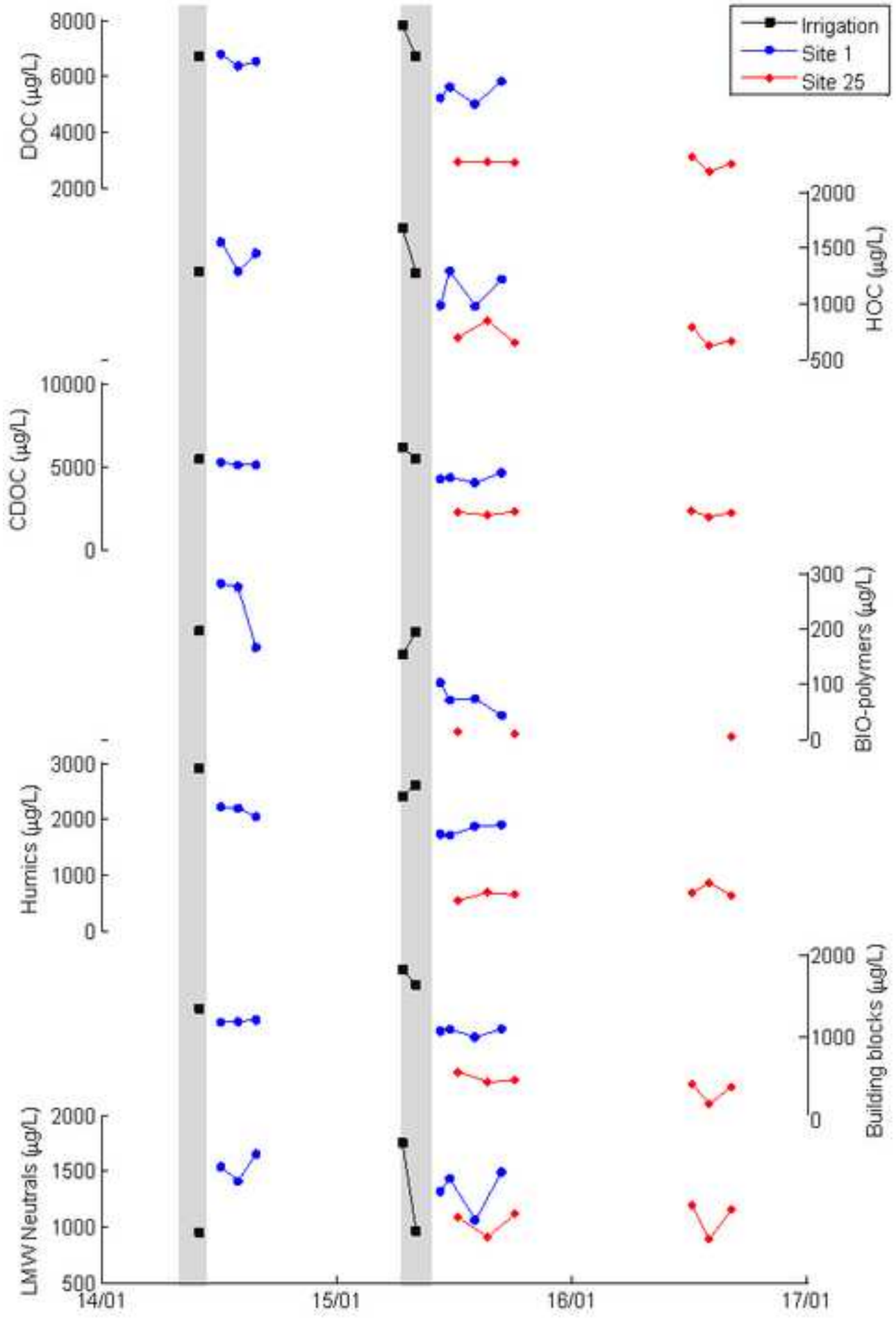

Figure5

Click here to download high resolution image

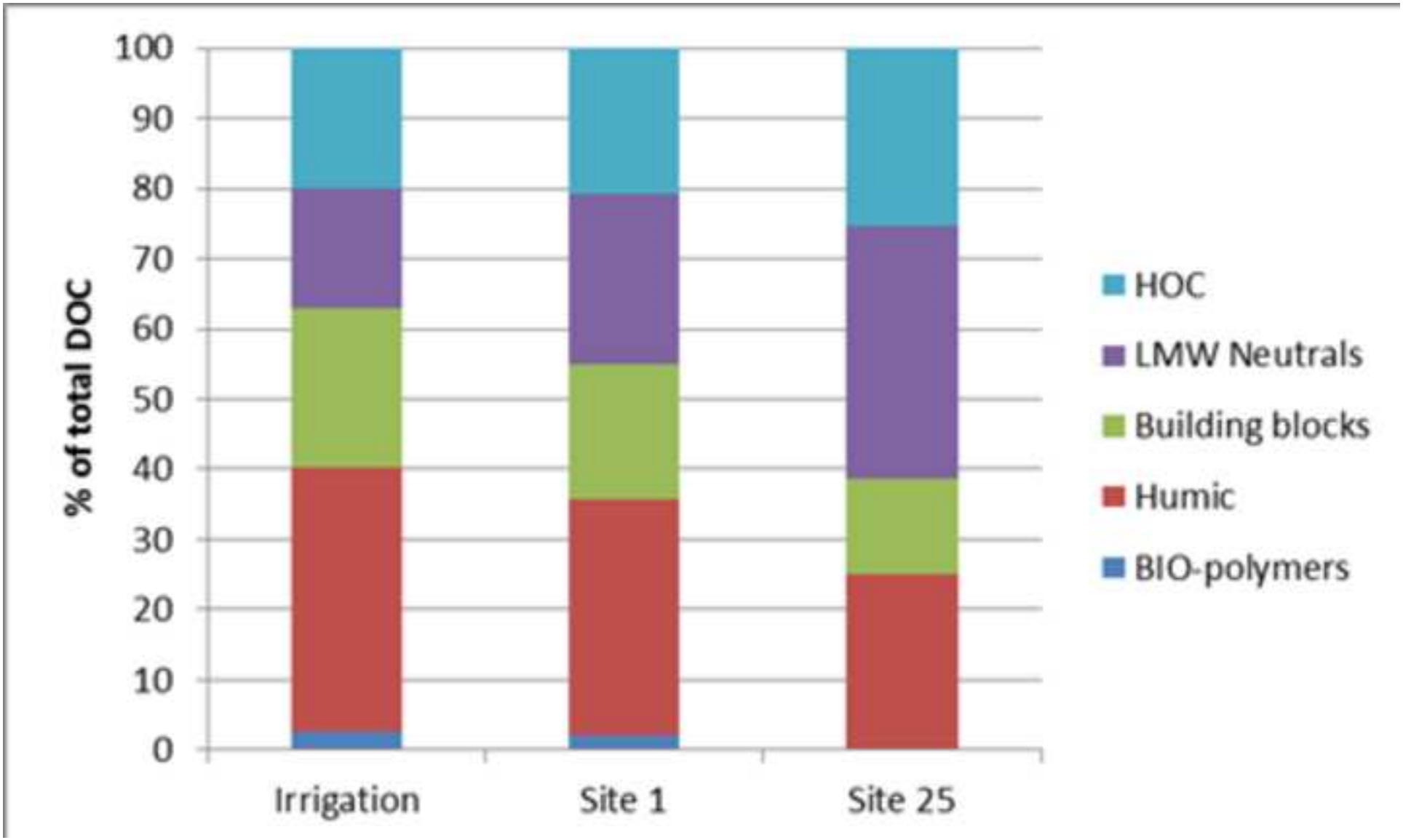

Figure6

Click here to download high resolution image

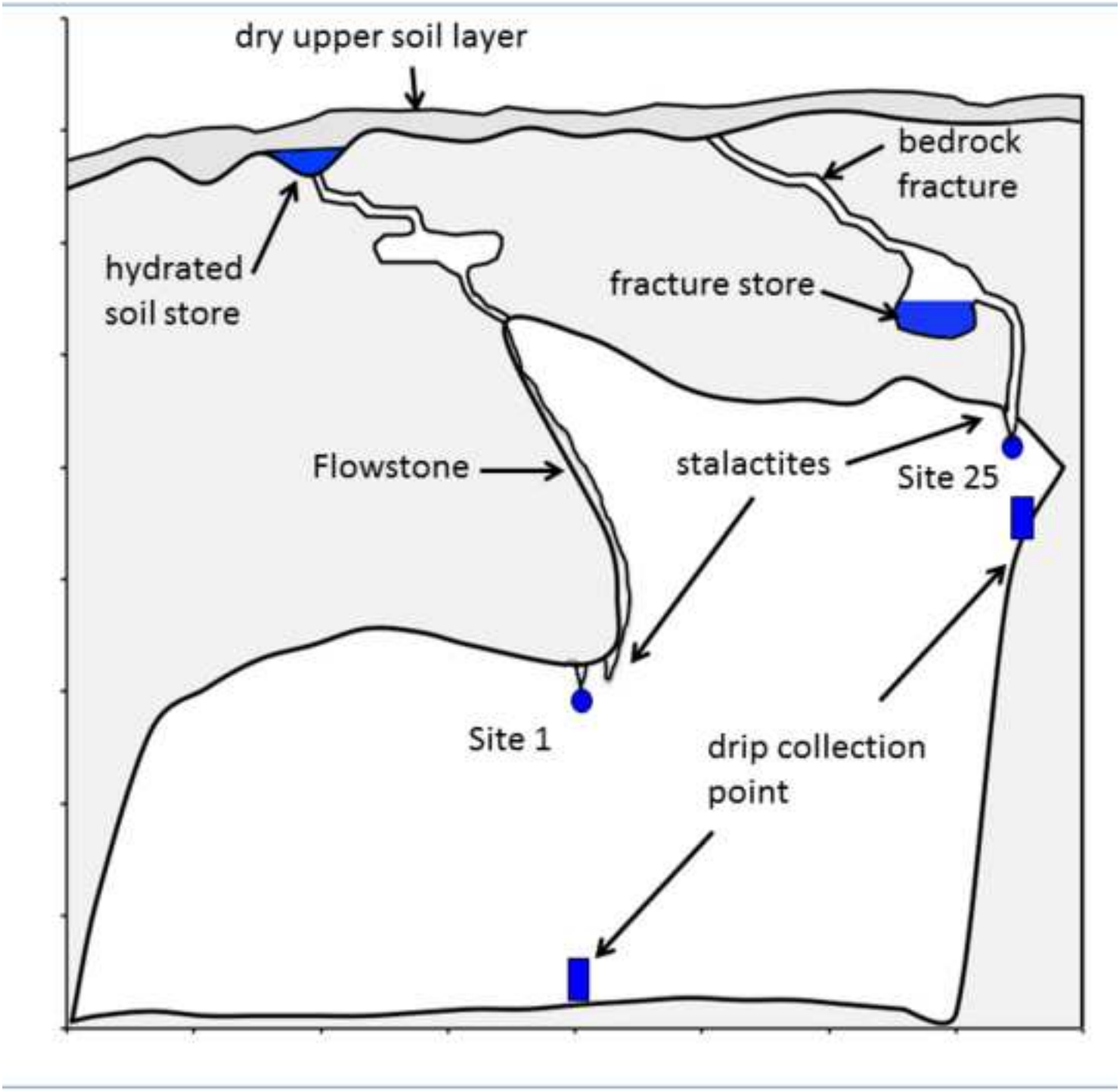

Figure7

Click here to download high resolution image

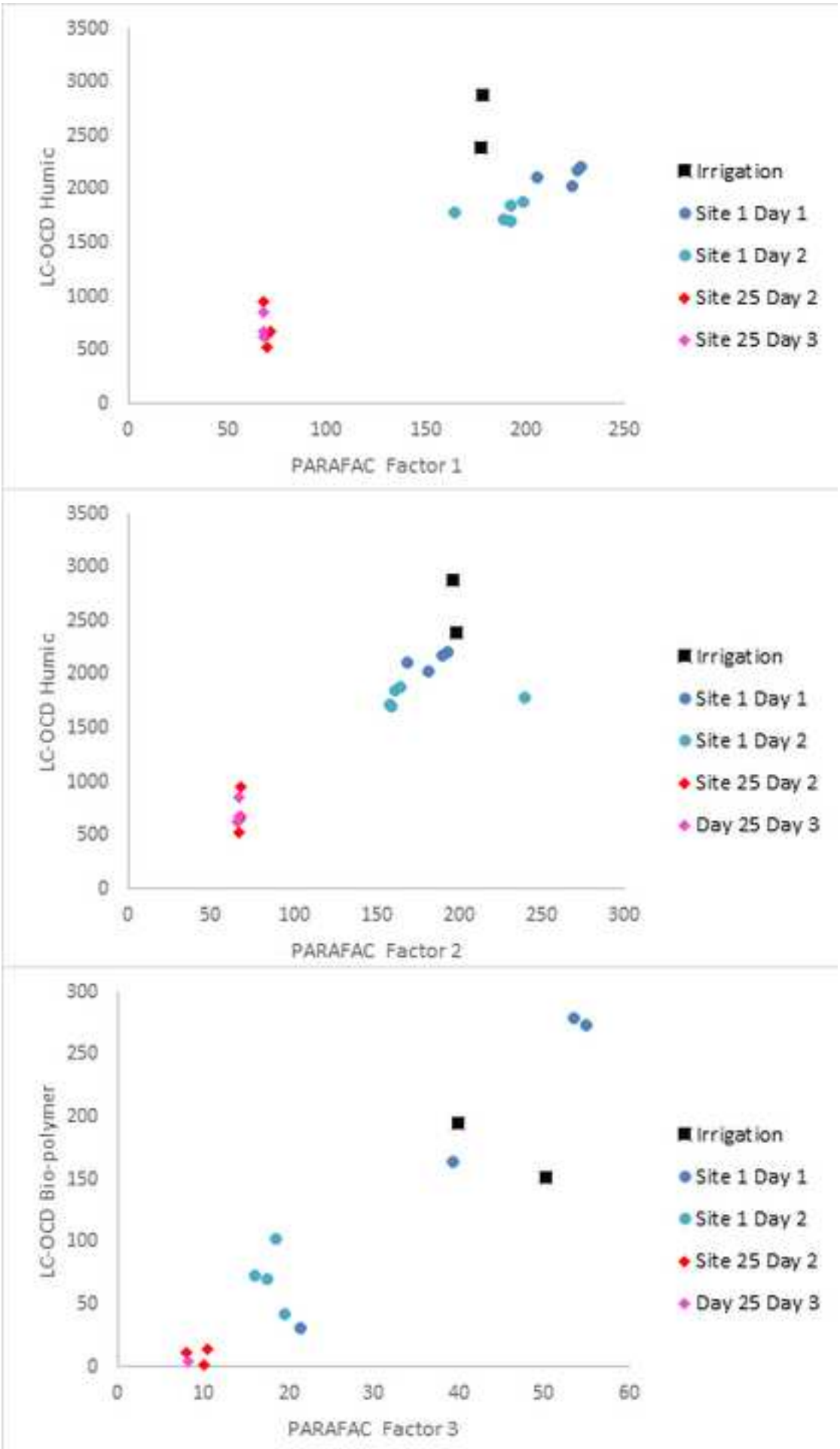

Figure8

Click here to download high resolution image

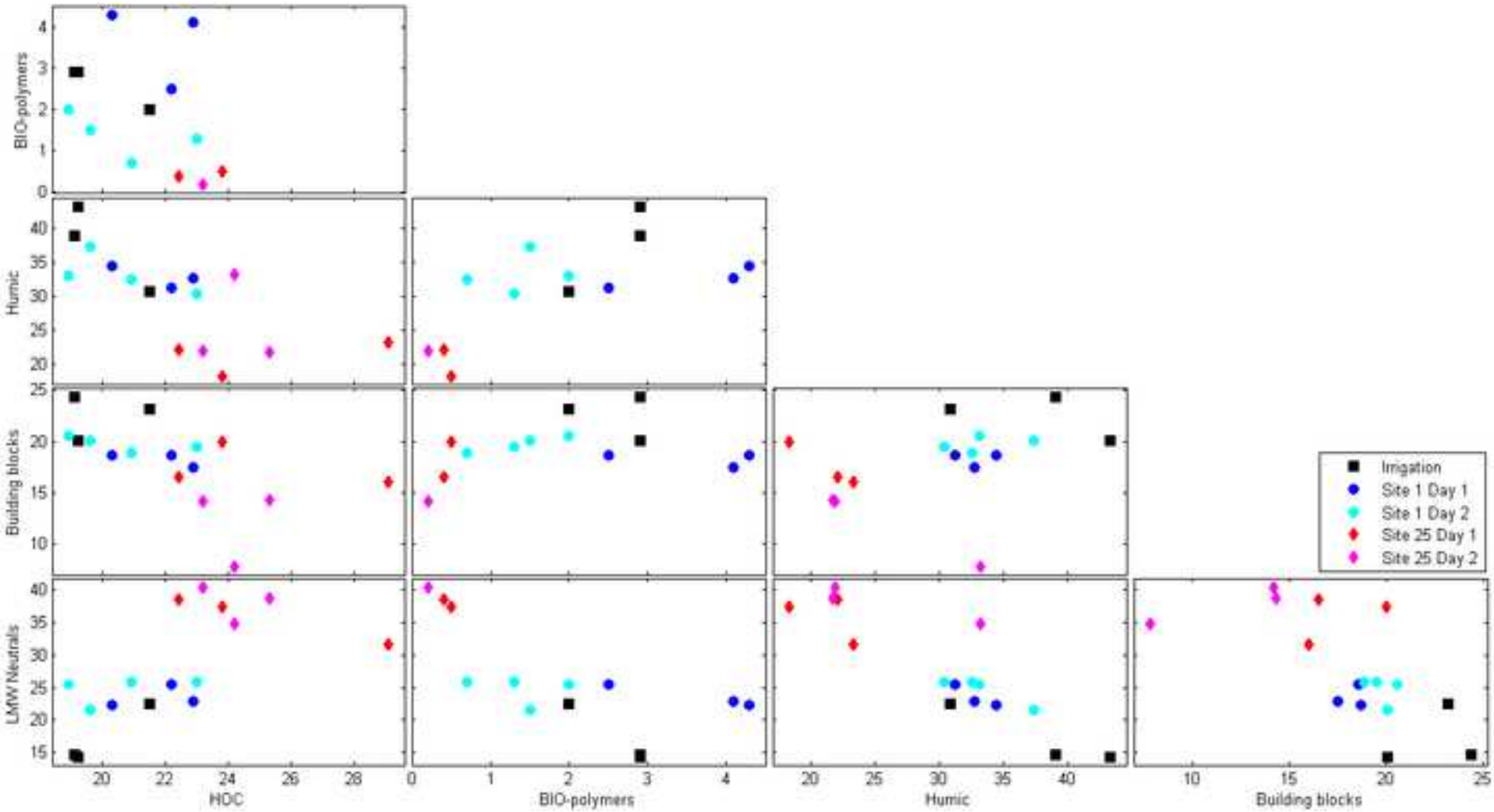

Figure9

Click here to download high resolution image

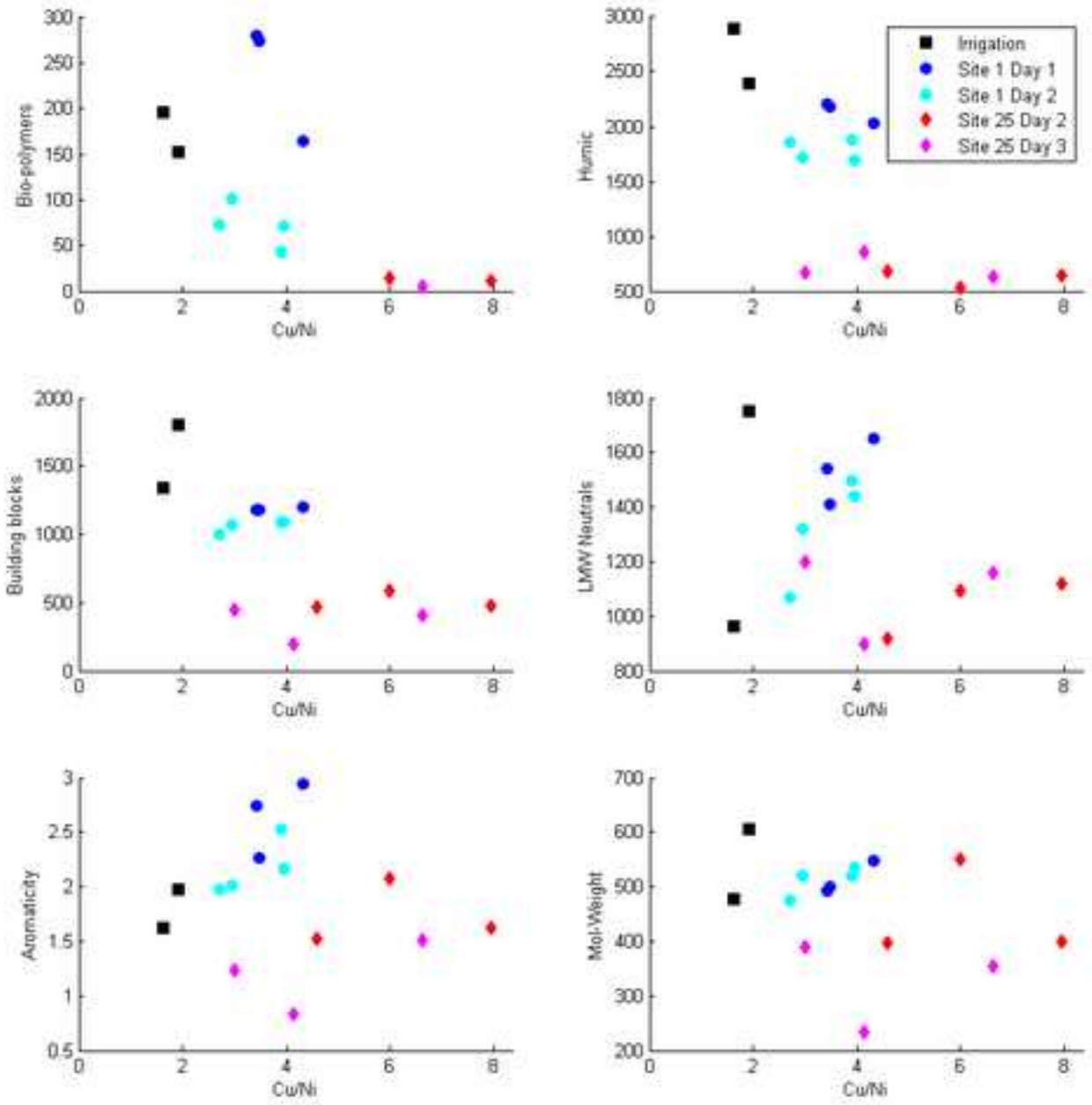

Supporting Data

Click here to download Electronic Annex: Supporting data.docx